Chemical Science

ROYAL SOCIETY OF CHEMISTRY

EDGE ARTICLE

View Article Online
View Journal | View Issue

Check for updates

Cite this: *Chem. Sci.*, 2024, **15**, 7206

All publication charges for this article have been paid for by the Royal Society of Chemistry

Experimental and theoretical comprehension of ESIPT fluorophores based on a 2-(2′-hydroxyphenyl)-3,3′-dimethylindole (HDMI) scaffold†

Timothée Stoerkler,‡[a] Gilles Ulrich,[a] Pascal Retailleau,[b] Adèle D. Laurent,[c] Denis Jacquemin *[cd] and Julien Massue *[a]

Excited-State Intramolecular Proton Transfer (ESIPT) emission is associated with intense single or multiple fluorescence in the solid-state, along with enhanced photostability and sensitivity to the close environment. As a result, ESIPT probes are attractive candidates for ratiometric sensing of a variety of substrates. A new family of ESIPT fluorophores is described herein, inspired by the well-known 2-(2'hydroxyphenyl)benzazole (HBX) organic scaffold. The connection of 3,3′-dimethylindole (or 3*H*-indole) derivatives with phenol rings triggers the formation of novel 2-(2′-hydroxyphenyl)-3,3′-dimethylindole (HDMI) fluorophores, capable of stimuli-responsive ESIPT emission. This brand new family of dyes displays redshifted emission, as compared to HBX, along with an unprecedented acid/base-mediated stabilization of different rotamers, owing to supramolecular interactions with methyl groups. These compounds are therefore highly sensitive to external stimuli, such as the presence of acid or base, where protonated and deprotonated species have specific optical signatures. Moreover, a new pyridine-functionalized HDMI dye displays acid-sensitive AIE properties. The photophysical properties of all compounds have also been studied using *ab initio* calculations to support experiments in deciphering the nature of the various radiative transitions observed and the related excited rotameric species.

Received 22nd March 2024
Accepted 16th April 2024

DOI: 10.1039/d4sc01937g

rsc.li/chemical-science

Open Access Article. Published on 16 April 2024. Downloaded on 5/17/2026 12:31:35 AM.
This article is licensed under a Creative Commons Attribution-NonCommercial 3.0 Unported Licence.

Introduction

The underlying rules of molecular fluorescence have been widely investigated, due to the importance of organic fluorophores in many applicative areas such as optoelectronics, biology, and luminescent displays.[1] It is well-known that both the nature and electronic functionalization of organic π-conjugated fluorescent scaffolds guide the key photophysical parameters, *i.e.*, emission wavelength (color), photoluminescent quantum yield, brightness, luminescent lifetime, and photostability.[2] Many organic dyes are fluorescent in dilute solution but the emission is typically lost in the solid-state, due to detrimental aggregation-caused quenching (ACQ) processes.[3] Rational design helped circumventing this issue by introducing steric hindrance to hamper aggregation[4] or developing molecular rotors, leading to emissive aggregates owing to the well-reported aggregation-induced emission (AIE) process.[5] In this context, Excited-State Intramolecular Proton Transfer (ESIPT) process,[6] relying on an ultrafast excited photo-tautomerism between enol (E*) and keto (K*) forms is an attractive alternative to engineer solid-state intense emission (Fig. 1a). Indeed, while ESIPT triggers detrimental molecular motions in the excited state which can quench the luminescence in solution, ESIPT dyes are typically characterized by a marked increase of emission intensity in solid, *e.g.*, in amorphous powder, aggregates, nanoparticles, or polymer thin films.[7] This trademark has long contributed to the use of ESIPT dyes as solid-state emitters in arrays of applications like organic light-emitting diodes,[8] security inks,[9] lasing,[10] and others.[11] ESIPT emission is also particularly attractive since it presents enhanced Stokes shifts limiting reabsorption processes and hampering inner-filter effect, leading to improved photostability of the dyes.[12] The rich photophysics of ESIPT dyes has been scrutinized and previous studies report the possibility to engineer partial frustration of the proton transfer process leading to dual E*/K* emission,[13] including panchromatic white emission in specific cases.[14] Complete frustration of

[a]*Institut de Chimie et Procédés pour l'Energie, l'Environnement et la Santé (ICPEES), Equipe Chimie Organique pour la Biologie, les Matériaux et l'Optique (COMBO), UMR CNRS 7515, Ecole Européenne de Chimie, Polymères et Matériaux (ECPM), 25 Rue Becquerel, 67087 Strasbourg Cedex 02, France. E-mail: massue@unistra.fr*

[b]*Service de Cristallographie Structurale, ICSN-CNRS, Université Paris-Saclay, 1 Avenue de la Terrasse, Bât. 27, 91198 Gif-sur-Yvette Cedex, France*

[c]*Nantes Université, CNRS, CEISAM UMR 6230, F-44000 Nantes, France*

[d]*Institut Universitaire de France (IUF), F-75005, Paris, France. E-mail: Denis.Jacquemin@univ-nantes.fr*

† Electronic supplementary information (ESI) available. CCDC 2260125 and 2260126. For ESI and crystallographic data in CIF or other electronic format see DOI: https://doi.org/10.1039/d4sc01937g

‡ Present address: University of Ottawa, Department of Chemistry, D'Iorio Hall, 10 Marie Curie, Ottawa ON Canada, K1N 6N5.

© 2024 The Author(s). Published by the Royal Society of Chemistry

Open Access Article. Published on 16 April 2024. Downloaded on 5/17/2026 12:31:35 AM.
This article is licensed under a Creative Commons Attribution-NonCommercial 3.0 Unported Licence.

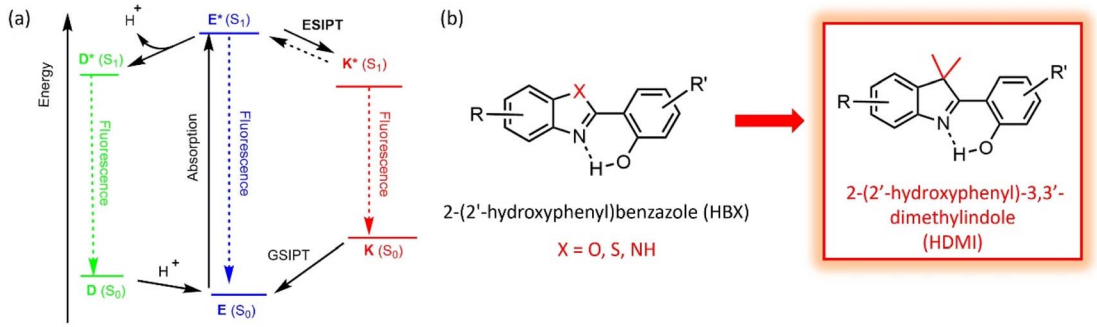

Fig. 1 (a) Schematic representation of ESIPT process and (b) structures of 2-(2′-hydroxyphenyl)benzazole (HBX) dyes and 2-(2′-hydroxyphenyl)-3,3-dimethylindole (HDMI).

ESIPT has also been evidenced in the case of important extension of the electronic conjugation which usually leads to strong solvatofluorochromic behavior of the E* tautomer.[15] Additionally, competition between ESIPT and deprotonation can be also observed in dissociative media where the presence of strongly fluorescent anions is characterized by a distinct D* emission band.[16] Recent developments have focused on building design rules to benefit from ESIPT luminescence both in solution and in solid with the same molecule.[17] These dual solution-solid emitters (called DSSE or DSE for dual-state emitters) arise either from a connection of ACQ and AIE moieties on the same scaffold,[18] an increase in molecular rigidity[19] or resonance-enhanced emission where the excited state is stabilized by a cyanine-like species.[20] For the latter case, our groups have recently reported pyridine- and pyridinium-substituted ESIPT dyes with a sensitivity to protonation.[21] All the above-listed characteristics have considerably contributed to the use of ESIPT luminescence for the engineering of environment-responsive fluorescent probes where the optical profile of the dyes can be subtly tuned by external stimuli, providing useful insights into the direct surroundings of the probes.[22] Over the years, a large number of molecular scaffolds has been reported to display ESIPT, typically composed of five- or six-membered H-bonded rings prone to undergo proton transfer in the excited state. Among these dyes, those derived from the 2-(2′-hydroxyphenyl)benzazole (HBX) family have been in the limelight owing to synthetic accessibility and photophysical versatility.[23] In particular, the nature of the heteroatom embedded in the benzazole heterocycle has been reported to strongly influence the photophysical parameters not only in terms of fluorescence color and intensity but also in its capacity to engineer stimuli-responsive multiple-state emission, by populating the various excited-state structures accessible in these dyes, typically E*, D*, and/or K* (Fig. 1a).[24] Building on these results, we started deeper investigations on the possibility to further modify the nature of the proton-acceptor to reach new electronic effects. Notably, 3,3′-dimethylindole (or 3*H*-indole) derivatives were studied in early 90's by Durocher *et al.*,[25] as promising building blocks for luminescent materials but have since remained unexplored. In this context, we report here on the synthesis, structural, and photophysical properties, along with *ab initio* calculations of novel HBX-derived fluorophores, called 2-(2′-hydroxyphenyl)-3,3′-dimethylindole (HDMI), where the heteroatom is replaced by a CMe_2 moiety, leading to a new family of 3,3′-dimethylindole-based dyes (Fig. 1b). To the best of our knowledge HDMI ESIPT dyes were not investigated before, though a theoretical investigation was performed on indoles (CH_2), revealing promising properties.[13b] We developed a series of fluorophores around the HDMI core with either ethynyl-extended fragments or pyridine-substituted derivatives. We notably show that in each case, substitution of the heteroatom by a CMe_2 leads to a marked redshift of the emission wavelength, along with the stabilization of a series of acid/base-mediated rotamers.

Results and discussion

Synthesis

The synthesis of unsubstituted HDMI dye **4**, pyridine-substituted HDMI dyes **6** and ethynyl-extended **7** is shown on Scheme 1. To allow evaluating the impact of CMe_2 insertion on the photophysical properties, the unsubstituted **HBX** dyes, along with the previously-reported bis-ethynyl HBX compounds **8–10** and HBO bis-pyridine dye **11** have also been included in this study (Scheme 1).[21a,24]

The 3,3′-dimethylindole core is synthesized in two steps, consisting of first a Friedel and Craft acylation of a phenol derivative with isobutyryl chloride and aluminum chloride, followed by a Fischer indole synthesis in the presence of phenylhydrazine, zinc chloride and magnesium sulfate. HDMI dyes **4** and **5** were obtained in 55–81% yields (Scheme 1). The presence of two bromine atoms on the phenol allowed the possibility of Pd-catalyzed cross-coupling reactions, either Suzuki–Miyaura-type to yield the pyridine-substituted HMDI derivative **6** or Sonogashira-type to provide the bis-ethynyl-extended HDMI derivative **7**. We underline that this choice of substitution was motivated by previous studies, in our groups, demonstrating the possibility to induce solution- and solid-state emission, by integrating similar moieties onto the core of HBX derivatives.[21,24]

X-ray diffraction

Single crystals of HDMI dyes **5** and **6** were obtained by slow evaporation of concentrated dichloromethane/methanol solutions. Planarity is strictly observed in the case of **5** with a platform lying in a crystallographic mirror plane perpendicular to the *b* axis (at $y = 1/4$ and $3/4$) of the monoclinic $P2_1/m$ unit cell

Open Access Article. Published on 16 April 2024. Downloaded on 5/17/2026 12:31:35 AM.
This article is licensed under a Creative Commons Attribution-NonCommercial 3.0 Unported Licence.

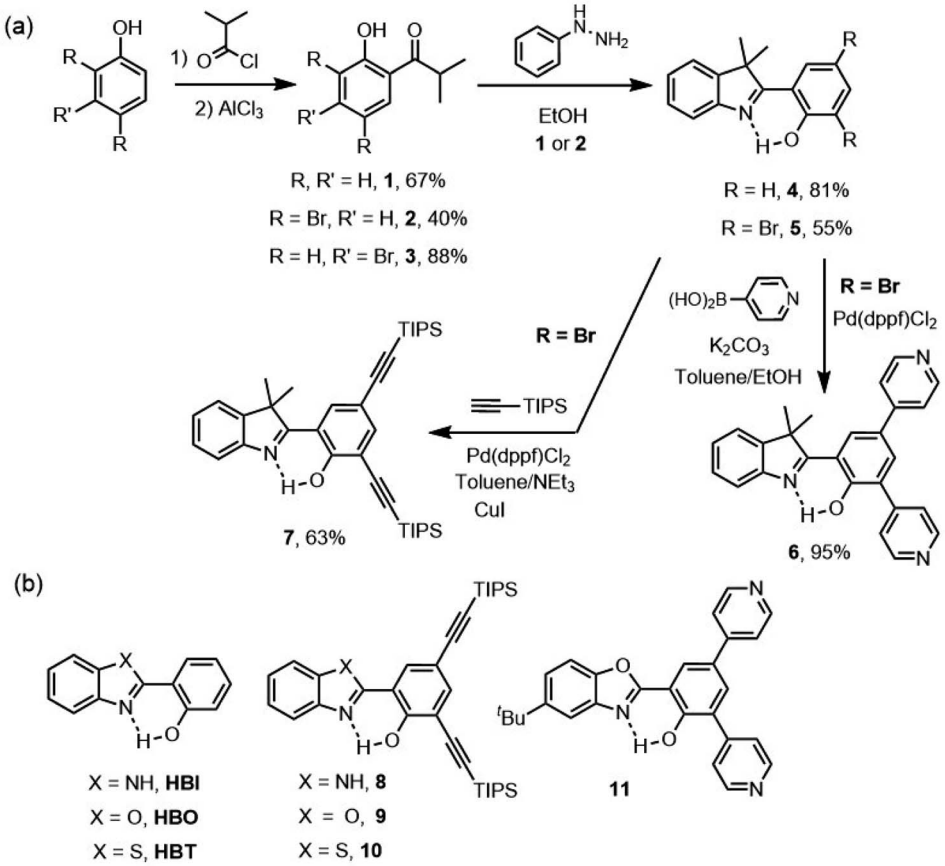

Scheme 1 (a) Synthesis of HDMI dyes **4**–**7**, (b) structures of unsubstituted HBX dyes and reported HBX dyes **8**–**11**.

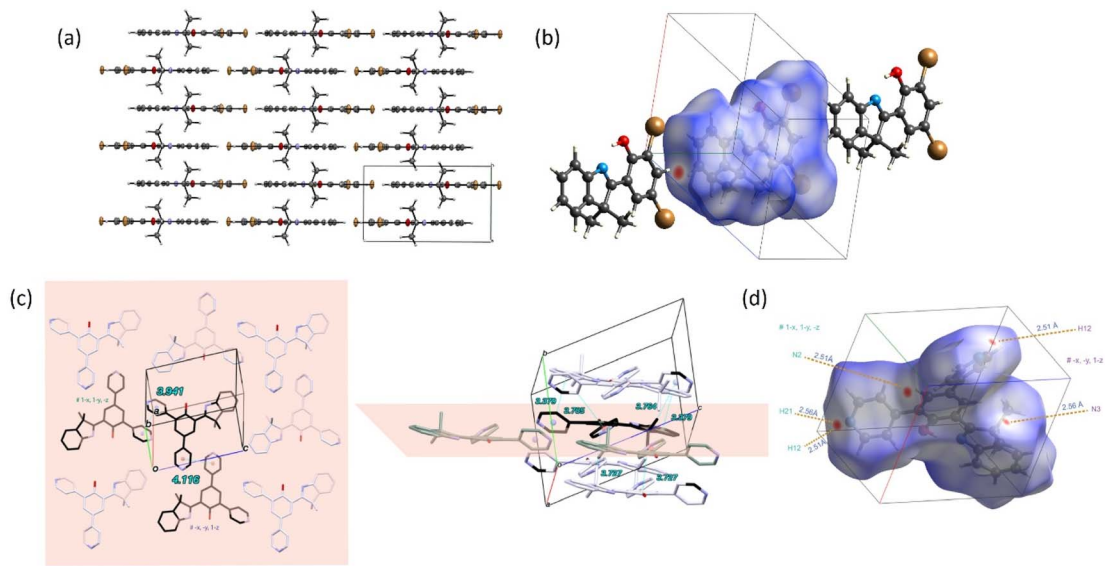

Fig. 2 (a) Molecular packing of HDMI **5** viewed down the *a* axis as layers parallel to *ac* plane, (b) Hirshfeld surface of HDMI **5**, mapped over d_{norm} in the color range −0.1965 to 1.0373 a.u, (c) view of the C–H···π with vicinal molecules (carbons in light grey) in the adjacent planes of HDMI **6** and the corresponding short contacts marked as red spots lying in the (−121) plane (in pink) (d) Hirshfeld surface of HDMI **6**, mapped over d_{norm} in the color range −0.0965 to 1.9102 a.u.

© 2024 The Author(s). Published by the Royal Society of Chemistry

Open Access Article. Published on 16 April 2024. Downloaded on 5/17/2026 12:31:35 AM. This article is licensed under a Creative Commons Attribution-NonCommercial 3.0 Unported Licence.

(Fig. 2a). Therefore, the interplanar distance between two molecular layers is $b/2 = 3.48$ Å, yet the shortest distance between the centroids of any cycle is over 4 Å. HDMI **5** molecules are all aligned along the [101] direction in one mirror plane (and inversely in the adjacent one). The Hirshfeld Surface (HS) analysis[26] and the associated two-dimensional fingerprint[27] were used to identify the close contacts present in a crystal by mapping of d_{norm} on the promolecule surface. The strength of the close contacts can be estimated qualitatively from the intensity of the red spots observed on the surface or *via* the $d_i + d_e$ contact distance as determined from a delineated fingerprint plot. The particularly short H···H contact is shown as a very intense red spot in the HS analysis for HDMI **5** (Fig. 2b) and the fingerprint plots for the more significant specific intermolecular interaction contributions to the surface (including the overall 2D fingerprint plot as the sum of the all-delineated plots), place this H···H major contribution on a par with those implying halogen contacts (together they represent 70% of the total contribution) (Fig. S12†). Nevertheless, the influence of π-stacking on the molecular layer packing cannot be ignored through the HS mapped of the shape-index and curvedness properties, even though the C/C contact contribution is 7% only (Fig. S13†). As for HDMI **6**, functionalized with two pyridine cycles, the platform shows a very slight curvature (13.3° dihedral angle between the phenol and the indole groups). The pyridine substituents at C11 and C13 of the phenol group (Fig. 2b) show dihedral angles of 41.8 and 35.0° respectively. HDMI **6** molecules are again arranged in wavy layers around the plane (−121) and the HS surface shows the closest contacts involving a triad of vicinal molecules (carbons in black, Fig. 2c) through N···H interactions. In addition, the pyridine groups are face to face but with centroid–centroid distances >4 Å. The interlayer C–H···π interactions provide a significant contribution to the HS (Fig. 2d), just after the prominent H···H interactions (almost half of the HS, Fig. S13†).

Photophysical properties

The photophysical properties of all HDMI dyes **4**, **6**, and **7**, along with unsubstituted **HBX** dyes and the previously reported HBX **8–11** have been studied in dilute solution, in dichloromethane and in the solid-state, as amorphous powders. The results are presented in Table 1, Fig. 4–7 and S15–S26.†

In order to evaluate the influence of the CMe_2 substitution, the photophysical properties of HDMI **4** and HDMI **7** were

Table 1 Photophysical data for HDMI **4**, **6**, **7**, unsubstituted **HBX** and HBX **8–11** in solution and in the solid-state

Dye	Solvent	λ_{abs}[a] (nm)	$\varepsilon \times 10^{-3}$ (M^{-1} cm^{-1})	λ_{em}[b] (nm)	ΔS[c] (cm^{-1})	QY[d]	τ[e] (ns)	K_r[f] (10^8 s^{-1})	K_{nr}[f] (10^8 s^{-1})
HBI	CH_2Cl_2	320	30.0	467	9800	0.03	3.8	0.08	2.55
	Solid	320[g]	—	466	9800	0.59	—	—	—
HBO	CH_2Cl_2	321	8.9	495	10 900	0.02	0.3	0.07	3.3
	CH_2Cl_2/HCl	321	20.1	494	10 900	0.03	0.1	3.00	97.0
	CH_2Cl_2/NBu_4OH	389	17.0	451	3500	0.65	0.1	65.0	35.0
	Solid	347[g]	—	501	8900	0.56	—	—	—
HBT	CH_2Cl_2	343	12.9	528	10 200	0.01	0.1	1.00	99.0
	Solid	340[g]	—	513	9900	0.49	—	—	—
HDMI **4**	CH_2Cl_2	349	12.5	464/519	7100	0.01	0.3	0.33	33.0
	CH_2Cl_2/HCl	393	12.9	476	4400	0.04	0.1	4.00	96.0
	CH_2Cl_2/NBu_4OH	411	3.9	512	4800	0.16	3.4	0.47	2.47
	Solid	340[g]	—	518	10 000	0.09	—	—	—
HDMI **6**	CH_2Cl_2	367	16.2	537	8600	0.09	0.2	4.50	45.5
	CH_2Cl_2/H^+	367	20.5	535	8600	0.21	3.9	0.53	2.03
	CH_2Cl_2/NBu_4OH	367/460	23.7	532	8600	0.58	3.4	1.71	1.24
	Solid	360[g]	—	574	10 400	0.11	—	—	—
HBO **11**	CH_2Cl_2	347	14.9	520	9600	0.58	4.3	1.35	0.97
	CH_2Cl_2/H^+	341	17.7	511	9800	0.56	4.1	1.37	1.07
	CH_2Cl_2/NBu_4OH	356/429	18.7	496	7900	0.48	4.3	1.12	1.21
	Solid	345	—	541	10 500	0.20	—	—	—
HDMI **7**	CH_2Cl_2	382	9.5	580(555)[h]	8900	0.04	0.2	2.00	48.0
	CH_2Cl_2/H^+	383	5.6	536	7500	0.06	0.4	1.50	23.5
	CH_2Cl_2/NBu_4OH	382/458	4.5	538	7600	0.45	4.8	0.94	1.15
	Solid	380[g]	—	583	9200	0.09	—	—	—
HBO **9**	CH_2Cl_2	367	13.6	533(516)[h]	8500	0.37	4.1	0.91	1.54
	CH_2Cl_2/H^+	367	11.9	539	8600	0.43	4.1	1.05	1.39
	CH_2Cl_2/NBu_4OH	433	19.1	482	2400	0.61	6.2	0.98	0.63
	Solid	360[g]	—	532	9000	0.38	—	—	—
HBT **10**	CH_2Cl_2	373	14.8	566(553)[h]	9200	0.18	2.2	0.82	3.73
	Solid	360[g]	—	574	10 300	0.20	—	—	—
HBI **8**	CH_2Cl_2	362	17.7	504(490)[h]	7800	0.67	5.1	1.31	0.65
	Solid	360[g]	—	495	7600	0.46	—	—	—

[a] Absorption maximum wavelength ($C = 10^{-5}$ M). [b] Emission maximum wavelength recorded at 25 °C ($C = 10^{-6}$ M for solution measurements). [c] Stokes shift. [d] Quantum yield in solution, using rhodamine 6G as a reference ($\lambda_{exc} = 488$ nm, $\Phi = 0.88$ in ethanol); quantum yield in the solid-state, as absolute (calculated with an integration sphere). [e] Luminescent lifetime. [f] k_r (10^8 s^{-1}) and k_{nr} (10^8 s^{-1}) were calculated using: $k_r = \Phi_F/\tau$, $k_{nr} = (1 - \Phi_F)/\tau$ where τ is the lifetime. [g] Excitation wavelength. [h] Emission maximum wavelength recorded at 77 K in MeTHF.

Open Access Article. Published on 16 April 2024. Downloaded on 5/17/2026 12:31:35 AM. This article is licensed under a Creative Commons Attribution-NonCommercial 3.0 Unported Licence.

studied and compared to their reported HBX analogs, *i.e.*, either unsubstituted or functionalized at the 3,5 positions of the phenol ring by ethynyl-extended tri(isopropyl)silyl (TIPS) groups. This substitution was chosen based on our previous report describing the introduction of triple bonds on the H-donor side of HBX dyes as a simple way to reduce detrimental non-radiative deactivations caused by the presence of a low-lying conical intersection between the ground and the excited states related to the twist around the interring bond after ESIPT took place.[19b] The photophysical data of HBO **11** (ref. 21*a*) are also reported in Table 1 for comparison purposes with HDMI **6**.

HDMI dye **4** presents a rather broad absorption band with a maximum absorption wavelength centered at 349 nm in solution in dichloromethane. This value represents a marked (slight) bathochromic shift as compared to its **HBI** and **HBO** (**HBT**) analogs. The absorption coefficients remain in the same range for all four compounds (ε = 7100–10200 M^{-1} cm^{-1} for HDMI **4**/**HBX**, see Fig. S15†). After excitation in the lowest-energy band, an intense single or dual emission band is recorded in solution. Indeed, while the HBX series a single K* emission band is present spanning from 467 to 528 nm, depending on the nature of the heteroatom with λ_{em} (**HBI**) > λ_{em} (**HBO**) > λ_{em} (**HBT**), the introduction of a 3*H*-indole heterocycle leads to a K* emission at 519 nm, similar to the one of HBT (Fig. 3a). As can be seen in Fig. S30,† the K* geometry of **HBO** is perfectly planar, whereas in **4**, one notes a small deformation around the inter-ring (formally double) bond, which might partially account for the redshift. Interestingly, one also notices on the experimental spectrum an additional band at 464 nm, that cannot be attributed to the enol, and whose nature remains elusive at this stage (see Theoretical calculations below). Expectedly, unsubstituted HBX dyes and related HDMI **4** are weakly fluorescent in solution, owing to pronounced molecular motions triggered by ESIPT (QY = 0.01–0.03, Fig. 3a).

In order to shed further light on the nature of the emissive shoulder observed at 464 nm, emission spectra of **4** in acidic (by bubbling HCl_g in CH_2Cl_2 solution) and basic (by adding an excess of NBu_4OH in CH_2Cl_2 solution) conditions were recorded (Fig. 3b). After protonation of **4**, a redshifted absorption band appears at 393 nm with a similar molar absorption coefficient (ε = 12 800 M^{-1} cm^{-1}, see Fig. S17†). Photoexcitation in this band leads to a single emission at 476 nm (QY = 0.04); a position relatively similar to the 464 nm shoulder observed above. In the protonated form, ESIPT is no more possible, consistent with the rather small Stokes shift value (4400 cm^{-1}) that is observed. We conclude that the additional emission band in CH_2Cl_2 could originate from the protonation of the 3,3′-dimethylindole scaffold, owing to higher pK_a/pK_{a*} values than the benzazole moiety, leading to push–pull species between indolium and phenol. In basic conditions, a new absorption band at 416 nm (ε = 3900 M^{-1} cm^{-1}) is observed, consistent with the presence of a phenolate in the ground state. After photoexcitation in this band, a single emission at 512 nm (QY = 0.16) is recorded. The strong increase of the QY value reflects a structural stabilization of the molecule in the excited state. The moderate Stokes shift (4600 cm^{-1}) logically indicates the absence of ESIPT (since there

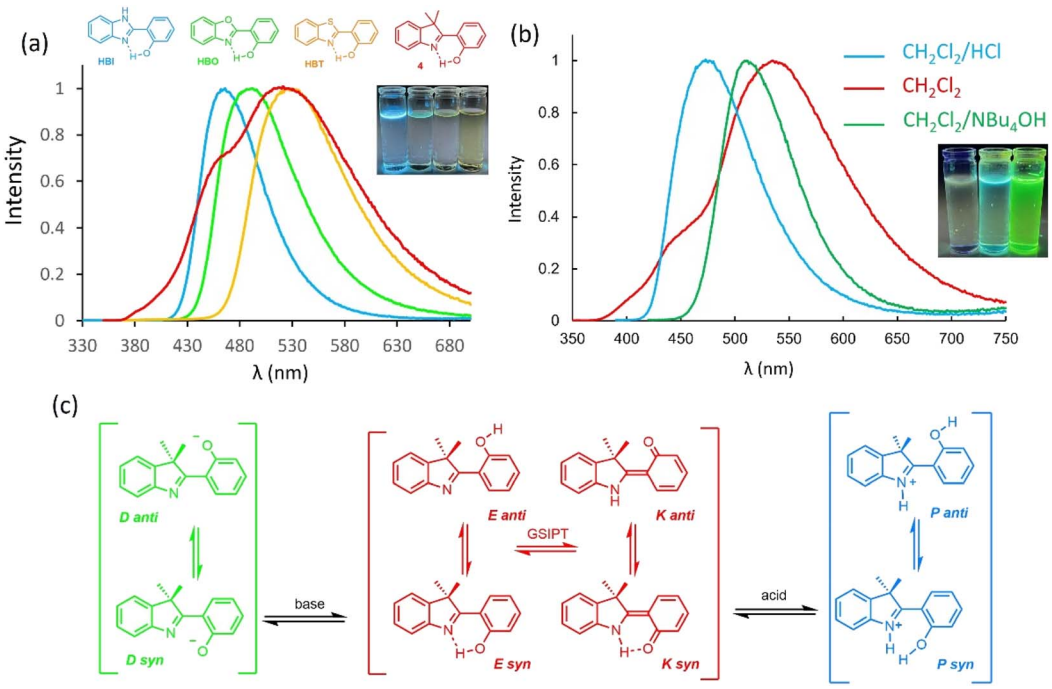

Fig. 3 (a) Normalized emission spectra in CH_2Cl_2 recorded at 25 °C of **HBI** (blue), **HBO** (green), **HBT** (orange) and HDMI **4** (red) dyes (λ_{exc} = 320–340 nm) (concentration: 1 μM). (Insets: photographs of CH_2Cl_2 solutions of **HBI**, **HBO**, **HBT** and HDMI **4** (from left to right) under irradiation (λ_{exc} = 365 nm)), (b) emission spectra of **4** in neutral CH_2Cl_2 (red) and after bubbling of HCl_g (blue) or addition of NBu_4OH (green) (Insets: photographs of neutral, acidic and basic CH_2Cl_2 solutions of HDMI **4** (from left to right) under irradiation (λ_{exc} = 365 nm)) and (c) *syn* and *anti* conformations of the neutral, protonated and deprotonated forms of HDMI **4**.

© 2024 The Author(s). Published by the Royal Society of Chemistry

Open Access Article. Published on 16 April 2024. Downloaded on 5/17/2026 12:31:35 AM. This article is licensed under a Creative Commons Attribution-NonCommercial 3.0 Unported Licence.

is no acidic proton left), but rather a charge transfer band resulting from a stabilized push–pull conformation (indole-phenolate). The Full Width at Half Maximum (FWHM) values can be estimated at 4500, 3800 and 2900 nm^{-1} for the neutral, acidic and basic forms of **4**, respectively.

In order to rationalize the photophysical properties of HDMI **4**, one hypothesis would be that two methyl groups of the 3,3′-dimethylindole are capable of stabilizing the phenolic proton or the phenolate anion, thus resulting in several species and conformations (Fig. 3c).[28]

These rotamers can be represented under the *syn* and *anti* nomenclature, depending on the relative position of the phenol (or phenolate) relative to the nitrogen of the indole. Four rotamers can be potentially found in the ground-state, *i.e.* E *syn*/E *anti*/K *syn* and K *anti* in the event of an unlikely GSIPT process (see Theory below). Similar rotations can help stabilize excited species with the occurrence of ESIPT. Additionally, cationic and anionic species can also undergo rotation to yield *syn* and *anti* rotamers. Based on these considerations and additional experiments, it is relatively safe to state that the high-energy band observed at 464 nm for HDMI **4** stems from a partial protonation of the indole ring.

To further investigate the intriguing photophysics of the HDMI scaffold, the bis ethynyl-extended HMDI **7** was synthesized and its optical properties studied and compared to its HBX analogs (Fig. 4). HDMI dyes **7** presents a broad absorption band with maximum absorption wavelengths centered at 382 nm in dichloromethane. As for HDMI **4**, this value is redshifted, as compared to their HBX counterparts (λ_{abs} = 362–373 nm for HBX **8–10**, Fig. S16†). The absorption coefficients remain in the same range (ε = 7800–9200 M^{-1} cm^{-1} for HMDI **7**/HBX **8–10**). Upon photoexcitation, HDMI **7** presents a single emission band at 580 nm, significantly redshifted as compared to HBX **8–10** (λ_{em} = 504–566 nm, Fig. 4a). These observations highlight the impact of the nature of the H-acceptor aza-heterocycle on the energy gap of the S_1–S_0 radiative transition of ESIPT fluorophores; a feature already investigated on HBX **8–10**.[24] As already reported,[19b] introducing ethynyl-extended substitution results in a marked increase of the fluorescent quantum yield in solution, yielding relatively bright dyes (QY = 0.67, 0.37, and 0.18 for **8–10**, respectively). While this trend does apply to HDMI **7**, which shows a four-fold increase of its quantum yield compared to the parent **4**, the dye remains poorly emissive (QY = 0.04 for **7** *vs.* 0.01 for **4**) in contrast to **8–10**, suggesting that the presence of a CMe_2 group somehow counterbalances the beneficial impact of ethynyl spacers in reducing the accessibility of non-radiative decay routes after ESIPT. To further understand the excited-state dynamics occurring in HDMI dyes, additional experiments were carried out. First, the fluorescence of ethynyl-extended derivatives, *i.e.*, HBX **8–10** and HDMI **7** was recorded in a glassy MeTHF matrix at 77 K (Fig. 4b). As expected, in all cases a significant blueshift in emission is observed (λ_{em} = 490–555 nm) with a strong enhancement of fluorescence intensity. We underline that this trend is more pronounced in the case of HDMI **7** compared to the HBX series, hinting at detrimental motions in this case. Furthermore, an important structuration of the fluorescence bands is recorded, consistent with the absence of molecular rotations in frozen solutions. The solid-state properties of **7–10** were also recorded as amorphous powders (Fig. 4c). All dyes present significant emission intensity in the solid-state with emission wavelengths spanning the 495–583 nm range with enhanced quantum yields (0.09–0.46). As mentioned before, a strong solid-state emission is indeed a trademark of ESIPT dyes.[7] Protonation/deprotonation studies were also performed on HDMI **7** and HBO **9** (Fig. S22–S25†). Protonation of both dyes does not modify the absorption wavelength nor the absorption coefficient, whereas deprotonation triggers the appearance of a redshifted absorption band in both cases (λ_{abs} = 485 and 433 nm for **7** and **9**, respectively), consistent with the formation of the phenolate species (Fig. S22 and S24†). However, photo-excitation of protonated species leads to different behaviors; while for HBO **9**, a fluorescence band at a maximum wavelength similar to the neutral case is observed (λ_{em} = 533–539 nm),

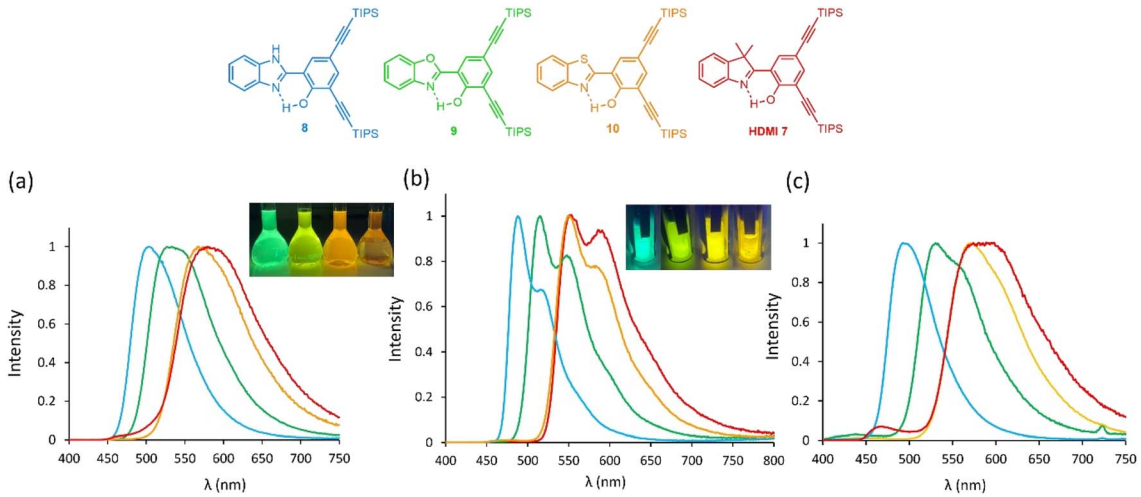

Fig. 4 Normalized emission spectra of HBI **8** (blue), HBO **9** (green), HBT **10** (orange) and HDMI **7** (red) recorded in (a) CH_2Cl_2 at 25 °C, (b) MeTHF at 77 K (concentration: 1 μM) and (c) in the solid-state, as embedded in 1% wt of KBr pellets.

Open Access Article. Published on 16 April 2024. Downloaded on 5/17/2026 12:31:35 AM. This article is licensed under a Creative Commons Attribution-NonCommercial 3.0 Unported Licence.

protonation of HDMI **7** leads to a significant blueshift of the emission (λ_{em} = 580 *vs.* 536 nm for the neutral and protonated forms of **7**, respectively). This is in line with the easier formation of the indolium ring *vs.* benzoxazolium, owing to higher pK_a/pK_{a*} values. Deprotonation of the phenol ring with Bu_4NOH leads in both cases to the observation of a highly emissive phenolates species with distinct wavelengths (λ_{em} = 538 nm, QY = 0.45 *vs.* 482 nm, QY = 0.61 for the anions **7** and **9**, respectively).

The introduction of pyridine moieties on the core of HBO-based ESIPT derivatives led to a stabilization of the excited state through resonance effects and a significant enhancement of the radiative rate constants in solution.[21] The absorption and emission spectra of HDMI dyes **6**, functionalized by two pyridine rings have been recorded in neutral and protonated dichloromethane as well as in basic conditions (Fig. 5b and S20†). For comparison purposes, the optical data of HBO **11**, functionalized with similar substitution has been superimposed on the spectra (Fig. 6a and S21†). For both dyes **6** and **11**, a single absorption band is observed in neutral conditions (λ_{abs} = 367 nm and 347 nm, respectively) whereas upon protonation, a significant hyperchromic effect is observed, with very little modification of the maximum absorption wavelength. In basic conditions, an additional redshifted absorption appears (λ_{abs} = 460 nm), consistent with the formation of the phenolate. Upon excitation of **11** in neutral conditions, a single band is observed at 520 nm (Δ_{SS} = 9600 cm^{-1}), which could presumably correspond to the decay of the anionic D* species, formed upon deprotonation.[21] Indeed, the photobasic nature of the pyridine moiety triggers deprotonation of the phenolic proton and the subsequent stabilization of the phenolate species by resonance effects through electronic delocalization. However, in the case of **6**, TD-DFT calculations helped pointing out a different scenario, that is absence of phenolic deprotonation by pyridine and the occurrence of ESIPT to observe emission at 537 nm stemming from the *syn*-K* tautomer (see below).

Upon protonation of **11**, the formation of the bis-pyridinium moieties hampers deprotonation, favoring ESIPT (K* transition) followed by formation of a stabilized merocyanine species. A slight blueshift is observed for the fluorescence band (λ_{em} = 511 nm), reminiscent of previous observations.[21] In the case of **6**, triple protonation being unlikely to occur due to electrostatic repulsions, unlike **4** and **7**, the formation of indolium is not observed. Instead, a single fluorescence band corresponding to the K* *syn* tautomer of the bis-pyridinium moieties is observed at 535 nm. In basic conditions, for **11**, formation of the phenolate, without the possibility of stabilization *via* the

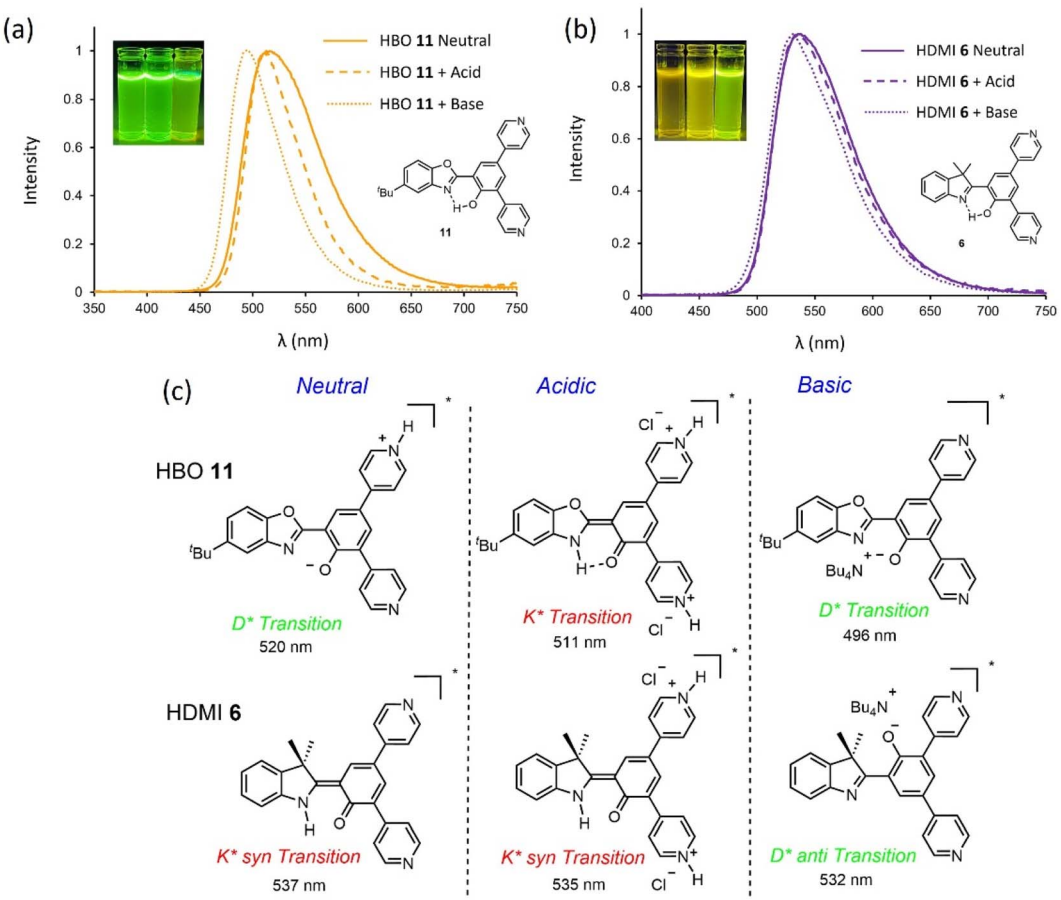

Fig. 5 Normalized emission spectra of (a) HBO **11** and (b) HDMI **6** in dichloromethane (neutral, plain; protonated with HCl_g, dashed and deprotonated with Bu_4NOH, dotted) (concentration: 1 μM) and (c) possible excited species for **11** and **6** in neutral, acidic and basic conditions.

© 2024 The Author(s). Published by the Royal Society of Chemistry

Open Access Article. Published on 16 April 2024. Downloaded on 5/17/2026 12:31:35 AM. This article is licensed under a Creative Commons Attribution-NonCommercial 3.0 Unported Licence.

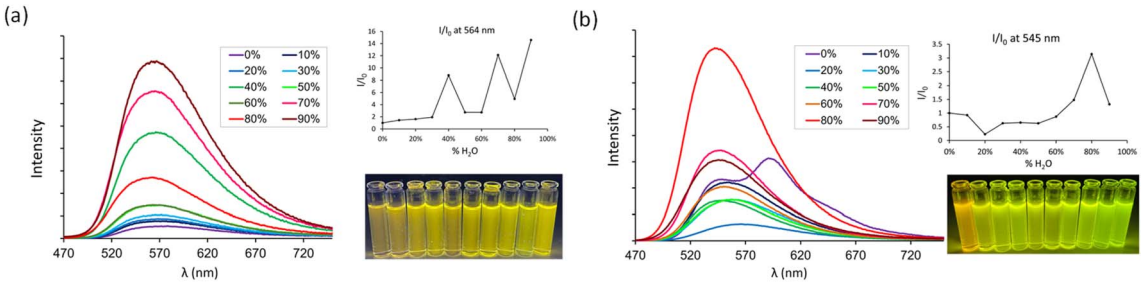

Fig. 6 Normalized emission spectra in THF/H_2O mixtures (0% to 90% H_2O) for (a) HDMI **6** in neutral dichloromethane and (b) HDMI **6.2H**$^+$ in protonated dichloromethane (λ_{exc} = 360 nm). (Concentration: 1 μM). Insets: Variation of I/I_0 (AIEE coefficient) at a given water percentage and photographs of THF/H_2O solutions under irradiation (λ_{exc} = 365 nm).

formation of a merocyanine species triggers a blueshift of the D* emission band (λ_{em} = 496 *vs.* 511 nm). Finally, the formation of the anionic species of HDMI **6** leads to the observation of the D* anti fluorescence (see calculations below).

It is important to stress that for both **6** and **11**, protonation and deprotonation act as external stimuli leading to a switch in terms of radiative transitions (D* *vs.* K*) but also emissive nature of rotamers (syn *vs.* anti) (Fig. 5c).

The HDMI series shows pronounced fluorescence quenching in solution as compared to their HBX analogs which we assign, at least partially, to easier rotational deactivations in the excited state (see Theoretical calculations below). To further investigate these effects experimentally, we decided to study their Aggregation-Induced Enhanced Emission (AIEE) properties. HDMI **6** was chosen as a representative example. The formation of emissive aggregates in THF/H_2O mixtures, with a concentration of **6** of around 10 μM, in neutral but also protonated conditions was scrutinized (Fig. 6). Both pyridine and pyridinium derivatives follow similar trends that is, a general increase of the fluorescence intensity along with the addition of water. However, their AIE coefficient is sensibly different: in its neutral state HDMI **6** displays significant AIE properties with a coefficient enhancement of 15.2, while upon protonation this value drops down to 3.1. This least rotational degree observed upon protonation could be correlated to the different QY observed previously in dichloromethane solution for **6** and **6.2H**$^+$ (QY = 0.09 *vs.* 0.21).

Ab initio calculations

To deeper understand the optical properties of the investigated HDMI compounds, we have modelled their properties of the excited states with *ab initio* methods (see the SI for all computational details) using time-dependent DFT (TD-DFT) combined to second-order coupled-cluster (CC2) simulations for the transition wavelengths. Our key results are summarized in Table 2. See Tables S2 and S3 in the ESI† for extra data and comparisons of theoretical and experimental wavelengths.

Let us start by HDMI **4**, and the corresponding model systems, **HBI**, **HBO**, and **HBT**. First, we have estimated the H-bond strength in the E* form for all four compounds (see Fig. S31 in the ESI†), and found strong H-bond in all four compounds in their lowest excited state (13–18 kcal mol^{-1}), the

Table 2 Key theoretical data for the investigated dyes: vertical absorption and emission wavelengths (in nm), difference of free energies between the keto and enol form in the excited-state (in eV), as well as the ESIPT barrier, *i.e.*, the difference of excited-state free energy between the enol and transition state (in eV). The transition wavelengths are determined with the cLR^2 solvent model (CH_2Cl_2) and include CC2 corrections, whereas the relative free energies are directly coming from the frequency calculations performed on the optimal LR-PCM-TD-DFT structures. See the ESI for details

Dye	λ_{abs}^{vert} (E) (nm)	λ_{fl}^{vert} (E*/D*) (nm)	λ_{fl}^{vert} (K*) (nm)	$\Delta G^{K^*-E^*}$ (eV)	$\Delta G^{TS^*-E^*}$ (eV)
HDMI **4**	327	399	505	−0.28	−0.06[b]
Protonated	353	442			
Deprotonated	444	517			
HBI	300	345	440	−0.37	−0.03[b]
HBO	300	348	448	−0.22	0.02
HBT	316	371	479	−0.27	−0.04[b]
HDMI **6**	345	[a]	529	[a]	[a]
(di)Protonated	356	[a]	524	[a]	[a]
Deprotonated	469	544			
HDMI **7**	351	[a]	538	[a]	[a]
HBI **8**	327	376	481	−0.52	−0.04[b]
HBO **9**	327	379	496	−0.44	−0.04[b]
HBT **10**	341	412	532	−0.41	−0.03[b]

[a] During the TD-DFT optimization, the E* form transforms into the K* spontaneously. [b] These values are obtained after true (TD-DFT) TS* optimization of the ESIPT. Some values are negative, indicating non-existing barrier, which is due to the thermodynamic and vibrational corrections. On the total energy scale, the TS* is, of course, higher in energy than the E*.

Open Access Article. Published on 16 April 2024. Downloaded on 5/17/2026 12:31:35 AM. This article is licensed under a Creative Commons Attribution-NonCommercial 3.0 Unported Licence.

strongest interaction being computed for HDMI **4**. In all four molecules, considered in their neutral form, theory predicts that the K* tautomer is much more stable than its E* counterpart, by values of at least −0.2 eV. According to previous calculations,[13,14] this is a clear indication that ESIPT should be the primary photophysical event after photon absorption. This conclusion is reinforced by the computed excited-state proton-transfer barriers[29] that are either negative (no barrier on the free energy scale) or extremely small (<0.02 eV) indicating quantitative ESIPT. This is also in line with a purely theoretical work devoted to H-indoles, showing that they are particularly prone to ESIPT.[13b] This analysis can be further corroborated by two findings. First, the electron density difference (EDD) representations, displayed in Fig. S27,† show that photon absorption yields significant decrease (increase) of electronic density on the hydroxyl (accepting nitrogen atom); a situation clearly leading to changes of the relative acidities of the two groups in a direction favorable to trigger ESIPT. Second, although vibronic effects are not accounted for in our calculations, we note that the vertical fluorescence wavelengths determined theoretically for both tautomers clearly indicate a better match with measurements for a K* fluorescence, *e.g.*, the experimental emission of HDMI **4** appears at 519 nm in CH_2Cl_2, which matches the computed value for the K* form (505 nm), but clearly not the one for the E* tautomer (399 nm), the latter corresponding to a 0.72 eV shift compared to the measurement, which would be an unexpectedly large error for the selected level of theory (CC2).

To obtain a more complete overview of the photophysics of HDMI **4**, we provide a graphical summary in Fig. 7. For both the neutral and protonated structures, the *syn* conformer is significantly more stable in both ground and excited states. According to theory, the absorption of the protonated structure is redshifted by +26 nm as compared to the (neutral) enol, whereas the fluorescence of the cationic derivative is blueshifted by −63 nm as compared to the keto neutral one. The corresponding experimental values are +44 nm and −43 nm, respectively. Interestingly, the deprotonated structure appears to be more stable in the *anti* form with the phenolate interacting with the two methyl groups of the indole moiety, an interaction that cannot take place in **HBO** nor **HBT**. This stabilizing interaction is present in both the ground and excited states (Fig. 7), ensuring that the deprotonated **4** is relatively rigid, consistent with its good quantum yield. Furthermore, in the Theoretical calculations, the D derivative shows a strongly redshifted absorption as compared to E, whereas the emission wavelengths of D* and K* are very similar, which fits the experimental trends well (see Table 1).

To rationalize the very low quantum yield of HDMI **4**, *ca.* 1% experimentally, we have performed a relaxed scan of the S_1 PES of the K* tautomer around the twisting coordinate. The result is displayed in Fig. S28,† and it turns out that at 90° a structure more stable than K* form by *ca.* −0.16 eV is obtained. This structure presents a very low transition energy (<1.3 eV) combined with a negligible oscillator strength ($f < 0.001$). It is either a dark state that would go back very quickly to the ground state non-radiatively (energy gap law) or a conical intersection not properly described by TD-DFT. In any case, it is clear that twisting around the interring bond in the K* tautomer results in emission quenching. As can be seen in Fig. S28,† a small "protective barrier" exists, of *ca.* 0.06 eV (at *ca.* 42°), which is sufficient to allow detecting emission, but insufficient to allow a bright fluorescence. In the same way, we compare the twisting potentials for the lowest excited state of **4** in its K*, P*, and D* forms (Fig. S28†). Clearly much larger barriers are found for both P* (0.37 eV, at *ca.* 90°) and D* (0.44 eV, at *ca.* 75°) than K*,

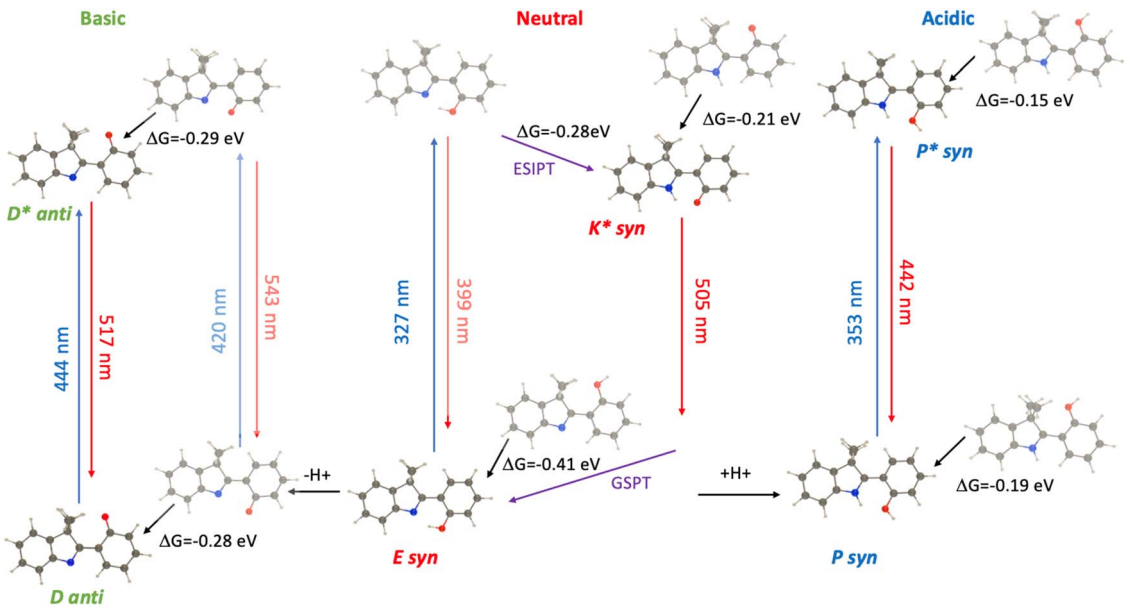

Fig. 7 Representation of the photophysical processes in HDMI **4** in CH_2Cl_2 as determined by theory. When possible, we provide the relative free energies between various species. The notation of the derivatives that are observed experimentally is given (see Fig. 3), whereas the shaded structures and transitions are not observed.

© 2024 The Author(s). Published by the Royal Society of Chemistry

Open Access Article. Published on 16 April 2024. Downloaded on 5/17/2026 12:31:35 AM. This article is licensed under a Creative Commons Attribution-NonCommercial 3.0 Unported Licence.

making the twisting mechanism much less accessible in these structures, which qualitatively explains the trends of the emission yields listed in Table 1 for HDMI **4** in various media.

Let us now turn towards HDMI **7** and its HBX analogs (HBI **8**, HBO **9** and HBT **10**). Here again, the calculations indicate a clear preference for the keto tautomers in the excited state; an effect enhanced with respect to the unsubstituted structures (see Table 2). For HDMI **7**, the TD-DFT geometry optimization starting the optimal ground-state E structure even spontaneously yields ESIPT during the excited-state minimization. Trying to locate the E* form of **7**, we have first performed a constrained optimization (freezing the OH distance to its S_0 value and optimizing all other parameters), followed in a second step by a full optimization starting from that structure. This also led to a K* geometry, clearly hinting that ESIPT takes place. This quantitative ESIPT in dyes **7–10** is also consistent with the EDD plots in Fig. S26† and the computed fluorescence energies in Table 2. Note that theory correctly restores the measured ordering of the emission wavelengths in the **7–10** series, as well as the experimental redshifts when going from the unsubstituted to the ethynyl-TIPS structures, albeit with an undershot magnitude for HDMI **7**. In Fig. S29,† we provide excited-state scans around the interring dihedral angle for the K* of HDMI **7** and HBO **9**. For the former, the barrier to the orthogonal form is noticeably increased as compared to HDMI **4**, from 0.06 to 0.19 eV, and the 90° degree becomes less stable (by *ca.* 0.15 eV) than its planar K* counterpart. As for **4**, this orthogonal structure is associated with a very low excitation energy and a negligible oscillator strength, so crossing the moderate 0.19 eV barrier would yield emission quenching. Nevertheless, this significant increase of the protective barrier qualitatively explains the four-fold increase of emission yield in going from HDMI **4** to **7**. It is noteworthy the situation becomes even more favorable in HBO **9** (Fig. S29†) in which the twisting yields a constant increase of energy (by *ca.* +0.51 eV from 0° to 90°) rendering this deleterious motion mostly ineffective, again in line with the experimental trend.

For HDMI **6**, theory predicts similar absorption wavelengths for the neutral and bis-protonated forms. This is a rather remarkable result, since the topology of the excited states of the two forms significantly differs, with a significant charge transfer to the pyridinium at the *ortho* position of the phenol in **6.2H$^+$**, whereas the pyridyl rings are rather passive moieties in the absorption **6** (Fig. S27†). For **6.2H$^+$**, we found as for HDMI **7**, a spontaneous ESIPT when optimizing the excited-state structure, with a fluorescence computed at 524 nm (Table 2), similar to the measured value of 535 nm. Finally, for the deprotonated form of HDMI **6**, we computed a strongly redshifted absorption but a similar fluorescence wavelength, as compared to the neutral and protonated structures, which is in agreement with the measurements, though theory cannot reproduce the exact ordering of the three close-lying emission bands.

Conclusions and outlook

Herein, we have described the design, multi-step synthesis, along with full structural and photophysical characterization of a novel family of fluorophores, prone to ESIPT, and based on the 2-(2′-hydroxyphenyl)-3,3′-dimethylindole (HDMI) scaffold. The presence of an indole ring, substituted by two methyl groups triggers major difference as compared to well-known HBX dyes. First, owing to methyl supramolecular stabilization, both *syn* and *anti* rotamers can be observed and the nature of the rotamers can be further mediated by acid and basic conditions. Second, the emission wavelength of these dyes is systematically bathochromically shifted, as compared to the equivalent HBX. Finally, they present AIE properties in neutral and acidic conditions. A full complementary theoretical study contributed to confirm the nature of the emissive transitions. These new dyes appear particularly sensitive to external stimuli and act as attractive candidates for the development of ratiometric sensors for a variety of targets. Work along these lines is currently under development in our groups.

Experimental section

Unsubstituted HBX dyes (**HBI**, **HBO**, **HBT**) are commercially available, while HBX **11–14** were synthesized according to a reported procedure.[24] Compounds **1** and **3** are already described in the literature.[30,31] Absorption data for HDMI **4** have been reported.[32]

General procedure for the synthesis of derivatives 1–3

The relevant phenol (1 mmol) was dissolved in isobutyryl chloride (0.15 mmol) and the reaction mixture was stirred for one hour at room temperature. Aluminum chloride (0.1 mmol) was then added and the resulting mixture heated at 130 °C for three hours. The brown sticky crude mixture diluted with diluted with 100 mL of ethyl acetate, extracted three times with 50 mL of ethyl acetate, washed with a brine solution, dried over $MgSO_4$ and concentrated *in vacuo*. The crude residue was purified by silica gel chromatography eluting with pet. Ether/EtOAc 10 : 0 to 9 : 1 to afford derivatives **1–3**.

Compound 1.[25] (110 mg, 67%). Colorless oil. ^{1}H NMR (400 MHz, $CDCl_3$) δ 12.45 (s, 1H), 7.72 (dd, ^3J = 8.1 Hz, ^4J = 1.7 Hz, 1H), 7.40 (ddd, ^3J = 8.3 Hz, ^3J = 7.2 Hz, ^4J = 1.7 Hz, 1H), 6.93 (dd, ^3J = 8.3 Hz, ^4J = 1.2 Hz, 1H), 6.83 (ddd, ^3J = 8.1 Hz, ^{3}J = 7.2 Hz, ^4J = 1.2 Hz, 1H), 3.55 (hept, ^3J = 6.8 Hz, 1H), 1.19 (d, ^3J = 6.8 Hz, 6H). ^{13}C NMR (101 MHz, $CDCl_3$) δ = 211.0, 163.3, 136.3, 130.0, 118.9, 118.9, 118.3, 35.1, 19.5.

Compound 2. (128 mg, 40%). White powder. ^{1}H NMR (500 MHz, $CDCl_3$) δ 13.14 (s, 1H), 7.87 (d, ^4J = 2.3 Hz, 1H), 7.85 (d, ^4J = 2.3 Hz, 1H), 3.54 (hept, J = 6.8 Hz, 1H), 1.26 (d, ^3J = 6.8 Hz, 6H). ^{13}C NMR (126 MHz, $CDCl_3$) δ = 209.8, 158.8, 141.3, 131.4, 119.7, 113.6, 110.4, 35.4, 19.3. HRMS (ESI-TOF) m/z: [M + H] Calcd for $C_{10}H_9Br_2O_2$: 318.8975; found, 318.8965.

Compound 3.[26] (214 mg, 88%). White powder. ^{1}H NMR (500 MHz, $CDCl_3$) δ 12.60 (s, 1H), 7.63 (d, ^3J = 8.6 Hz, 1H), 7.19 (d, ^4J = 2.0 Hz, 1H), 7.04 (dd, ^3J = 8.6 Hz, ^4J = 1.9 Hz, 1H), 3.53 (hept, ^3J = 6.8 Hz, 1H), 1.25 (s, 3H), 1.23 (s, 3H). ^{13}C NMR (126 MHz, $CDCl_3$) δ = 210.4, 163.8, 130.9, 130.6, 122.5, 122.1, 117.2, 35.3, 19.4.

General procedure for the synthesis of HDMI dyes 4–5

A mixture of isopropylphenylketone (1 mmol), phenylhydrazine hydrochloride (0.12 mmol), zinc chloride (0.01 mmol) and magnesium sulfate (1 mmol) in 15 mL of ethanol was heated

Open Access Article. Published on 16 April 2024. Downloaded on 5/17/2026 12:31:35 AM. This article is licensed under a Creative Commons Attribution-NonCommercial 3.0 Unported Licence.

under reflux for 15 hours. After cooling down, the mixture was filtered on cotton, quenched with 30 mL of $NaHCO_3$, and extracted with ethyl acetate three times. Organic layers were combined and washed with a brine solution, dried over $MgSO_4$, and concentrated *in vacuo*. The crude residues were purified by silica gel chromatography eluting with pet. Ether/CH_2Cl_2 10 : 0 to 8 : 2 to afford HDMI dyes **4–5**.

HDMI 4. (193 mg, 81%). Yellow oil. ^{1}H NMR (500 MHz, $CDCl_3$) δ 14.46 (s, 1H), 7.82 (dd, ^3J = 8.2 Hz, ^4J = 1.6 Hz, 1H), 7.64–7.58 (m, 1H), 7.44–7.34 (m, 3H), 7.34–7.27 (m, 1H), 7.16 (dd, ^3J = 8.4 Hz, ^4J = 1.2 Hz, 1H), 6.95 (ddd, J = 8.2, 7.2, 1.2 Hz, 1H), 1.67 (s, 6H). ^{13}C NMR (126 MHz, $CDCl_3$) δ = 184.8, 162.4, 150.3, 146.0, 132.9, 128.7, 128.1, 126.4, 121.2, 119.8, 118.6, 118.4, 115.7, 53.8, 25.3. HRMS (ESI-TOF) m/z: [M + H+] calcd for $C_{16}H_{16}NO$: 238.1226; found, 238.1223.

HDMI 5. (217 mg, 55%). Yellow solid. ^{1}H NMR (500 MHz, $CDCl_3$) δ 15.69 (s, 1H), 7.84 (d, ^4J = 2.3 Hz, 1H), 7.78 (d, ^4J = 2.3 Hz, 1H), 7.62–7.56 (m, 1H), 7.42–7.37 (m, 2H), 7.37–7.32 (m, 1H), 1.64 (s, 6H). ^{13}C NMR (126 MHz, $CDCl_3$) δ = 182.8, 158.4, 149.1, 145.9, 137.9, 129.9, 128.4, 127.2, 121.4, 120.2, 117.4, 113.5, 109.5, 53.8, 25.1. HRMS (ESI-TOF) m/z: [M + H+] calcd for $C_{16}H_{14}Br_2NO$: 393.9437; found, 393.9442.

Synthesis of HDMI 7

HDMI **5** (1 mmol), the corresponding alkyne (1.5 mmol per bromine atom) and Pd(dppf)Cl_2, (0.05 mmol) were dissolved in 20 mL of toluene/NEt_3 (4 : 1, v/v) and the solution was degassed with argon for 20 min. Copper iodide (0.1 mmol) was then added and the mixture stirred at 90 °C for 15 hours. The reaction was cooled down to room temperature, quenched with saturated NH_4Cl solution and the mixture was extracted three times with ethyl acetate. The organic layers were combined and washed with brine, dried with $MgSO_4$ before the solvents were removed *in vacuo*. The crude products were purified by a silica column chromatography eluting with pet. Ether/CH_2Cl_2 10 : 0 to 9 : 1 to yield HDMI dyes **7**, as a yellow powder (377 mg, 63%). ^{1}H NMR (500 MHz, $CDCl_3$) δ 15.42 (s, 1H), 7.84 (d, ^4J = 2.1 Hz, 1H), 7.64 (d, ^4J = 2.1 Hz, 1H), 7.61 (d, ^3J = 8.4 Hz, 1H), 7.42–7.36 (m, 2H), 7.34–7.30 (m, 1H), 1.64 (s, 6H), 1.19 (s, 21H), 1.16 (s, 21H). ^{13}C NMR (126 MHz, $CDCl_3$) δ = 183.7, 164.0, 149.8, 145.9, 139.6, 132.4, 128.3, 126.8, 121.3, 120.1, 115.6, 114.3, 113.2, 106.3, 102.0, 96.2, 89.3, 53.9, 25.3, 18.9, 18.9, 11.5. HRMS (ESI-TOF) m/z: [M + H$^+$] calcd for $C_{38}H_{56}NOSi_2$: 598.3895; found, 598.3886.

Synthesis of HDMI 6

In a Schlenk tube, HDMI **5** (1 mmol), 4-pyridinyl boronic acid (3 mmol) and potassium carbonate (4 mmol) were dissolved in 9 mL of toluene/ethanol (2 : 1). The resulting suspension was degassed with argon before the addition of Pd(dppf)Cl_2 (0.05 mmol) and the mixture was stirred at 95 °C for 15 hours. The reaction was cooled down to room temperature, quenched with saturated NH_4Cl solution and the mixture was extracted three times with ethyl acetate. The organic layers were combined and washed with brine, dried with $MgSO_4$ before the solvents were removed *in vacuo*. The crude product was purified by a silica column chromatography using CH_2Cl_2/EtOH (98 : 2) as eluent to yield HDMI **6** as a yellow powder in 95% yield (373 mg). ^{1}H NMR (500 MHz, $CDCl_3$) δ 15.69 (s, 1H), 8.76–8.69 (m, 4H), 8.14 (d, ^4J = 2.3 Hz, 1H), 7.76 (d, ^4J = 2.3 Hz, 1H), 7.67–7.65 (m, 2H), 7.61 (d, ^3J = 7.4 Hz, 1H), 7.55–7.52 (m, 2H), 7.44 (d, ^3J = 7.4 Hz, 1H), 7.41 (td, ^3J = 7.4 Hz, ^4J = 1.3 Hz, 1H), 7.36 (td, ^3J = 7.4 Hz, ^4J = 1.3 Hz, 1H), 1.76 (s, 6H). ^{13}C NMR (126 MHz, $CDCl_3$) δ = 184.2, 160.9, 150.8, 150.7, 149.9, 149.6, 147.5, 145.8, 145.7, 131.8, 129.2, 128.4, 128.4, 127.6, 127.1, 124.3, 121.5, 121.4, 121.2, 120.1, 116.7, 54.1, 25.5. HRMS (ESI-TOF) m/z: [M + H$^+$] calcd for $C_{26}H_{22}N_3O$: 392.1757; found, 392.1767.

Data availability

The data that support the findings of this study are available from the corresponding authors upon reasonable request.

Author contributions

T. S. designed the fluorophores, conducted all synthesis and most photophysical experiments. P. R. conducted X-Ray diffraction studies. A. D. L. and D. J. conducted all ab initio calculations and co-wrote the manuscript. G. U. contributed to discussing the results and J. M. conceptualized and supervised the project, contributed to photophysical experiments and wrote the manuscript.

Conflicts of interest

There are no conflicts to declare.

Acknowledgements

The authors thank the CNRS for financial support. T. S. acknowledges the Ecole Doctorale des Sciences Chimiques (ED 222) for a PhD fellowship. This work of the Interdisciplinary Institute HiFunMat, as part of the ITI 2021–2028 program of the University of Strasbourg, CNRS and Inserm, was supported by IdEx Unistra (ANR-10-IDEX-0002) and SFRI (STRAT'US project, ANR-20-SFRI-0012) under the framework of the French Investments for the Future Program. D. J. et A. D. L. thank the CCIPL/GliCID (*Centre de Calcul Intensif des Pays de la Loire*) installed in Nantes for generous allocation of computational time.

References

1 B. Valeur, *Molecular Fluorescence: Principles and Applications*, Wiley-VCH Verlag GmbH, 2001.

2 (*a*) D. Frath, J. Massue, G. Ulrich and R. Ziessel, Luminescent Materials: Locking π-Conjugated and Heterocyclic Ligands with Boron(III), *Angew. Chem., Int. Ed.*, 2014, **53**(9), 2290–2310; (*b*) J. Wu, Z. Shi, L. Zhu, J. Li, X. Han, M. Xu, S. Hao, Y. Fan, T. Shao, H. Bai, B. Peng, W. Hu, X. Liu, C. Yao, L. Li and W. Huang, The Design and Bioimaging Applications of NIR Fluorescent Organic Dyes with High Brightness, *Adv. Opt. Mater.*, 2022, **10**, 2102514; (*c*) H. Crawford, M. Dimitriadi, J. Bassin, M. T. Cook, T. Fedatto Abelha and J. Calvo-Castro, Mitochondrial Targeting and Imaging with

 © 2024 The Author(s). Published by the Royal Society of Chemistry

Open Access Article. Published on 16 April 2024. Downloaded on 5/17/2026 12:31:35 AM. This article is licensed under a Creative Commons Attribution-NonCommercial 3.0 Unported Licence.

Small Organic Conjugated Fluorophores: A Review, *Chem.–Eur. J.*, 2022, **28**, e2022023; (*d*) S. Wang, B. Li and F. Zhang, Molecular Fluorophores for Deep-Tissue Bioimaging, *ACS Central Sci*, 2020, **6**(8), 1302–1316.

3 (*a*) T. F. Excimers, *Angew. Chem., Int. Ed.*, 1969, **8**(5), 333–343; (*b*) M. Tasior, D. Kim, S. Singha, M. Krzeszewski, K. H. Ahn and D. T. Gryko, π-Expanded coumarins: synthesis, optical properties and applications, *J. Mater. Chem. C*, 2015, **3**, 1421–1446.

4 (*a*) M. Stolte, T. Schembri, J. Süß, D. Schmidt, A.-M. Krause, M. O. Vysotsky and F. Würthner, 1-Mono- and 1,7-Disubstituted Perylene Bisimide Dyes with Voluminous Groups at Bay Positions: In Search for Highly Effective Solid-State Fluorescence Materials, *Chem. Mater.*, 2020, **32**(14), 6222–6236; (*b*) P. Gawrys, O. Morawski, M. Banasiewicz and C. A. Barboza, Magnifying the ESIPT process in tris(salicylideneanilines) *via* the steric effect – a pathway to the molecules with panchromatic fluorescence, *Phys. Chem. Chem. Phys.*, 2023, **25**, 12500–12514.

5 J. Mei, N. L. Leung, R. T. Kwok, J. W. Lam and B. Z. Tang, Aggregation-Induced Emission: Together We Shine, United We Soar, *Chem. Rev.*, 2015, **115**, 11718–11940; Z. Zhao, H. Zhang, J. W. Y. Lam and B. Z. Tang, Aggregation-Induced Emission: New Vistas at the Aggregate Level, *Angew. Chem., Int. Ed.*, 2020, **59**, 9888–9907.

6 (*a*) J. Zhao, S. Ji, Y. Chen, H. Guo and P. Yang, Excited state intramolecular proton transfer (ESIPT): from principal photophysics to the development of new chromophores and applications in fluorescent molecular probes and luminescent materials, *Phys. Chem. Chem. Phys.*, 2012, **14**, 8803–8817; (*b*) J. Massue, D. Jacquemin and G. Ulrich, Molecular Engineering of Excited-state Intramolecular Proton Transfer (ESIPT) Dual and Triple Emitters, *Chem. Lett.*, 2018, **47**(9), 1083–1089.

7 (*a*) V. S. Padalkar and S. Seki, Excited-state intramolecular proton-transfer (ESIPT)-inspired solid state emitters, *Chem. Soc. Rev.*, 2016, **45**, 169–202; (*b*) T. Stoerkler, T. Pariat, A. D. Laurent, D. Jacquemin, G. Ulrich and J. Massue, Sterically Hindered 2-(2'-Hydroxyphenyl)benzoxazole (HBO) Emitters: Synthesis, Spectroscopic Studies, and Theoretical Calculations, *Eur. J. Org Chem.*, 2022, **30**, e202200661; (*c*) L. Chen, P.-Y. Fu, H.-P. Wang and M. Pan, Excited-State Intramolecular Proton Transfer (ESIPT) for Optical Sensing in Solid State, *Adv. Opt. Mater.*, 2021, **9**(23), 2001952.

8 (*a*) J. E. Kwon and S. Y. Park, Advanced Organic Optoelectronic Materials: Harnessing Excited-State Intramolecular Proton Transfer (ESIPT) Process, *Adv. Mater.*, 2011, **23**(32), 3615–3642; (*b*) M. Mamada, K. Inada, T. Komino, W. J. Potscavage Jr, H. Nakanotani and C. Adachi, Highly Efficient Thermally Activated Delayed Fluorescence from an Excited-State Intramolecular Proton Transfer System, *ACS Central Sci.*, 2017, **3**(7), 769.

9 Y. Zhang, H. Yang, H. Ma, G. Bian, Q. Zang, J. Sun, C. Zhang, Z. An and W.-Y. Wang, Excitation Wavelength Dependent Fluorescence of an ESIPT Triazole Derivative for Amine Sensing and Anti-Counterfeiting Applications, *Angew. Chem., Int. Ed.*, 2019, **58**, 8773–8778.

10 (*a*) J. Massue, A. Felouat, P. M. Vérité, D. Jacquemin, K. Cyprych, M. Durko, L. Sznitko, J. Mysliwiec and G. Ulrich, An extended excited-state intramolecular proton transfer (ESIPT) emitter for random lasing applications, *Phys. Chem. Chem. Phys.*, 2018, **20**, 19958–19963; (*b*) A. Shukla, V. T. Ngoc Mai, V. V. Divya, C. H. Suresh, M. Paul, V. Karunakaran, S. K. M. McGregor, I. Allison, K. N. Narayanan Unni, A. Ajayaghosh, E. B. Namdas and S.-C. Lo, Amplified Spontaneous Emission from Zwitterionic Excited-State Intramolecular Proton Transfer, *J. Am. Chem. Soc.*, 2022, **144**, 13499–13510; (*c*) M. Durko-Maciag, G. Ulrich, D. Jacquemin, J. Mysliwiec and J. Massue, Solid-State Emitters Presenting a Modular Excited-State Proton Transfer (ESIPT) Process: Recent Advances in Dual-State Emission and Lasing Applications, *Phys. Chem. Chem. Phys.*, 2023, **25**, 15085–15098.

11 P. Gayathri, M. Pannipara, A. G. Al-Sehemi and S. P. Anthony, Recent advances in excited state intramolecular proton transfer mechanism-based solid state fluorescent materials and stimuli-responsive fluorescence switching, *CrystEngComm*, 2021, **23**, 3771–3789.

12 N. N. M. Y. Chan, A. Idris, Z. H. Z. Abidin, H. A. Tajuddina and Z. Abdullah, White light employing luminescent engineered large (mega) Stokes shift molecules: a review, *RSC Adv.*, 2021, **11**, 13409–13445.

13 (*a*) E. Heyer, K. Benelhadj, S. Budzák, D. Jacquemin, J. Massue and G. Ulrich, On the Fine-Tuning of the Excited-State Intramolecular Proton Transfer (ESIPT) Process in 2-(2′-Hydroxybenzofuran)benzazole (HBBX) Dyes, *Chem.–Eur. J.*, 2017, **23**, 7324–7336; (*b*) C. Azarias, S. Budzák, A. D. Laurent, G. Ulrich and D. Jacquemin, Tuning ESIPT fluorophores into dual emitters, *Chem. Sci.*, 2016, **120**, 3763–3774.

14 K. Benelhadj, W. Muzuzu, J. Massue, P. Retailleau, A. Charaf-Eddin, A. D. Laurent, D. Jacquemin, G. Ulrich and R. Ziessel, White Emitters by Tuning the Excited-State Intramolecular Proton-Transfer Fluorescence Emission in 2-(2′-Hydroxybenzofuran)benzoxazole Dyes, *Chem.–Eur. J.*, 2014, **20**, 12843.

15 (*a*) M. Raoui, J. Massue, C. Azarias, D. Jacquemin and G. Ulrich, Highly fluorescent extended 2-(2′-hydroxyphenyl)benzazole dyes: synthesis, optical properties and first-principle calculations, *Chem. Commun.*, 2016, **52**(59), 9216–9219; (*b*) A. P. Demchenko, K.-C. Tang and P.-T. Chou, Excited-state proton coupled charge transfer modulated by molecular structure and media polarization, *Chem. Soc. Rev.*, 2013, **42**, 1379–1408; (*c*) M. Munch, E. Colombain, T. Stoerkler, P. M. Vérité, D. Jacquemin, G. Ulrich and J. Massue, Blue-Emitting 2-(2′-Hydroxyphenyl)benzazole Fluorophores by Modulation of Excited-State Intramolecular Proton Transfer: Spectroscopic Studies and Theoretical Calculations, *J. Phys. Chem. B*, 2022, **126**, 2108–2118.

16 (*a*) M. Munch, M. Curtil, P. M. Vérité, D. Jacquemin, J. Massue and G. Ulrich, Ethynyl-Tolyl Extended 2-(2′-Hydroxyphenyl)benzoxazole Dyes: Solution and Solid-state Excited-State Intramolecular Proton Transfer (ESIPT) Emitters, *Eur. J. Org Chem.*, 2019, 1134–1144; (*b*) K.-I. Sakai, T. Ishikawa and T. Akutagawa, A blue-white-

Open Access Article. Published on 16 April 2024. Downloaded on 5/17/2026 12:31:35 AM. This article is licensed under a Creative Commons Attribution-NonCommercial 3.0 Unported Licence.

yellow color-tunable excited state intramolecular proton transfer (ESIPT) fluorophore: sensitivity to polar-nonpolar solvent ratios, *J. Mater. Chem. C*, 2013, **1**(47), 7866–7871.

17 (*a*) A. Huber, J. Dubbert, T. D. Scherz and J. Voskuhl, Design Concepts for Solution and Solid-State Emitters–A Modern View point on Classical and Non-Classical Approaches, *Chem.–Eur. J.*, 2023, **29**, e2022024; (*b*) T. Stoerkler, T. Pariat, A. D. Laurent, D. Jacquemin, G. Ulrich and J. Massue, Excited-State Intramolecular Proton Transfer Dyes with Dual-State Emission Properties: Concept, Examples and Applications, *Molecules*, 2022, **27**, 2443; (*c*) J. L. Belmonte-Vazquez, Y. A. Amador-Sanchez, L. A. Rodriguez-Cortes and B. Rodriguez-Molina, Dual-State Emission (DSE) in Organic Fluorophores: Design and Applications, *Chem. Mater.*, 2021, **33**, 7160–7184.

18 Q. Huang, Q. Guo, J. Lan and J. You, Tuning the dual emission of keto/enol forms of excited-state intramolecular proton transfer (ESIPT) emitters *via* intramolecular charge transfer (ICT), *Dyes Pigm.*, 2021, **193**, 109497.

19 (*a*) K. Skonieczny, J. Yoo, J. M. Larsen, E. M. Espinoza, M. Barbasiewicz, V. I. Vullev, C.-H. Lee and D. T. Gryko, How To Reach Intense Luminescence for Compounds Capable of Excited-State Intramolecular Proton Transfer?, *Chem.–Eur. J.*, 2016, **22**, 7485–7496; (*b*) J. Massue, A. Felouat, M. Curtil, P. M. Vérité, D. Jacquemin and G. Ulrich, Solution and solid-state Excited-State Intramolecular Proton Transfer (ESIPT) emitters incorporating Bis-triethyl-or triphenylsilylethynyl units, *Dyes Pigm.*, 2019, **160**, 915–922.

20 (*a*) X. Liu, F. Zhao, B. Chen, Y. Huang, L. Xu, E. Li, L. Tan and H. Zhang, Resonance-Enhanced Emission Effects toward Dual-State Emissive Bright Red and Near-infrared Emitters, *Chem.–Eur. J.*, 2023, **29**, e202300381; (*b*) N. Suzuki, A. Fukazawa, K. Nagura, S. Saito, H. Kitoh-Nishioka, D. Yokogawa, S. Irle and S. Yamaguchi, A Strap Strategy for Construction of an Excited-State Intramolecular Proton Transfer (ESIPT) System with Dual Fluorescence, *Angew. Chem., Int. Ed.*, 2014, **53**, 8231–8235.

21 (*a*) T. Pariat, T. Stoerkler, C. Diguet, A. D. Laurent, D. Jacquemin, G. Ulrich and J. Massue, Dual Solution-/Solid-State Emissive Excited-State Intramolecular Proton Transfer (ESIPT) Dyes: A Combined Experimental and Theoretical Approach, *J. Org. Chem.*, 2021, **86**, 17606–17619; (*b*) T. Stoerkler, A. D. Laurent, G. Ulrich, D. Jacquemin and J. Massue, Influence of ethynyl extension on the dual-state emission properties of pyridinium-substituted ESIPT fluorophores, *Dyes Pigm.*, 2022, **208**, 110872.

22 (*a*) A. C. Sedgwick, L. Wu, H.-H. Han, S. D. Bull, X.-P. He, T. D. James, J. L. Sessler, B. Z. Tang, H. Tian and J. Yoon, Excited-state intramolecular proton-transfer (ESIPT) based fluorescence sensors and imaging agents, *Chem. Soc. Rev.*, 2018, **47**, 8842–8880; (*b*) T. Pariat, P. M. Vérité, D. Jacquemin, J. Massue and G. Ulrich, 2,2-Dipicolylamino substituted 2-(2′-hydroxybenzofuranyl)benzoxazole (HBBO) derivative: towards ratiometric sensing of divalent zinc cations, *Dyes Pigm.*, 2021, **190**, 109338.

23 (*a*) D. Yao, S. Zhao, J. Guo, Z. Zhang, H. Zhang, Y. Liu and Y. Wang, Hydroxyphenyl-benzothiazole based full color organic emitting materials generated by facile molecular modification, *J. Mater. Chem. C*, 2011, **21**, 3568–3570; (*b*) Y. Chen, Y. Fang, H. Gu, J. Qiang, H. Li, J. Fan, J. Cao, F. Wang, S. Lu and X. Chen, Color-Tunable and ESIPT-Inspired Solid Fluorophores Based on Benzothiazole Derivatives: Aggregation-Induced Emission, Strong Solvatochromic Effect, and White Light Emission, *ACS Appl. Mater. Interfaces*, 2020, **12**(49), 55094–55106; (*c*) V. R. Mishra, C. W. Ghanavatkar and N. Sekar, Towards NIR-Active Hydroxybenzazole (HBX)-Based ESIPT Motifs: A Recent Research Trend, *ChemistrySelect*, 2020, **5**, 2103–2113.

24 T. Pariat, M. Munch, M. Durko-Maciag, J. Mysliwiec, P. Retailleau, P. M. Vérité, D. Jacquemin, J. Massue and G. Ulrich, Impact of Heteroatom Substitution on Dual-State Emissive Rigidified 2-(2′-hydroxyphenyl)benzazole Dyes: Towards Ultra-Bright ESIPT Fluorophores, *Chem.–Eur. J.*, 2021, **27**(10), 3483–3495.

25 (*a*) M. Belletête, S. Nigam and G. Durocher, Conformational Analysis and Electronic Spectroscopy of Donor-Acceptor 3H-Indole, *J. Phys. Chem.*, 1995, **99**, 4015–4024; (*b*) S. Nigam, M. Belletête, R. S. Sarpal and G. Durocher, Proton transfer equilibrium reactions in donor-acceptor 3H-indole derivatives: electronic spectroscopy and photophysics of the neutral molecules and their charged species in water, *J. Lumin.*, 1995, 65–76; (*c*) M. Belletête and S. Nigam, G Durocher. Photophysics of some substituted 3H-indole probe molecules and their charged species, *Can. J. Chem.*, 1994, **72**, 2239.

26 M. A. Spackman and D. Jayatilaka, Hirshfeld surface analysis, *CrystEngComm*, 2009, **11**, 19–32.

27 J. J. McKinnon, D. Jayatilaka and M. A. Spackman, Towards quantitative analysis of intermolecular interactions with Hirshfeld surfaces, *Chem. Commun.*, 2007, 3814–3816.

28 R. D. Green, *Hydrogen Bonding by C-H Groups*, Red Globe Press, London, 1974.

29 (*a*) Y. Ma, Y. Yang, R. Lan and Y. Li, Effect of Different Substituted Groups on Excited-State Intramolecular Proton Transfer of 1-(Acylamino)-anthraquinons, *J. Phys. Chem. C*, 2017, **27**, 14779–14786; (*b*) Y. Zhao, Y. Ding, Y. Yang, W. Shi and Y. Li, Fluorescence deactivation mechanism for a new probe detecting phosgene based on ESIPT and TICT, *Org. Chem. Front.*, 2019, **6**, 597–602.

30 K. N. Tripathi, S. Singh, N. Akhtar, K. Manna and R. P. Singh, Visible-light-driven site-selective alkylation of the benzo core of coumarins, *Chem. Commun.*, 2022, **58**, 9674–9677.

31 S. R. Bollinger, D. W. Engers, J. D. Panarese, M. West, J. L. Engers, M. T. Loch, A. L. Rodriguez, A. L. Blobaum, C. K. Jones, A. Thompson Gray, P. J. Conn, C. W. Lindsley, C. M. Niswender and C. R. Hopkins, Discovery, Structure–Activity Relationship, and Biological Characterization of a Novel Series of 6-((1H-Pyrazolo[4,3-b]pyridin-3-yl)amino)-benzo[d]isothiazole-3-carboxamides as Positive Allosteric Modulators of the Metabotropic Glutamate Receptor 4 ($mGlu_4$), *J. Med. Chem.*, 2019, **62**(1), 342–358.

32 B. Robinson and M. Uppal Zubair, The Autoxidation of 2-(2-Hydroxyphenyl)-3-methylindol, *J. Chem. Soc.*, 1971, 976–977.

© 2024 The Author(s). Published by the Royal Society of Chemistry